Evidence of electronic cloaking from chiral electron transport in bilayer graphene nanostructures

Kyunghoon Lee,[1,2] Seunghyun Lee,[1,3] Yun Suk Eo,[4] Cagliyan Kurdak,[4] and Zhaohui Zhong[1,*]
[1]*Department of Electrical Engineering and Computer Science, University of Michigan, Ann Arbor, Michigan 48109, USA*
[2]*Department of Electrical Engineering and Computer Science, University of California, Berkeley, California 94720, USA*
[3]*Department of Electronics and Radio Engineering, Kyung Hee University, Gyeonggi 446-701, South Korea*
[4]*Department of Physics, University of Michigan, Ann Arbor, Michigan 48109, USA*
(Received 24 April 2016; published 14 November 2016)

The coupling of charge carrier motion and pseudospin via chirality for massless Dirac fermions in monolayer graphene has generated dramatic consequences, such as the unusual quantum Hall effect and Klein tunneling. In bilayer graphene, charge carriers are massive Dirac fermions with a finite density of states at zero energy. Because of their non-relativistic nature, massive Dirac fermions can provide an even better test bed with which to clarify the importance of chirality in transport measurement than massless Dirac fermions in monolayer graphene. Here, we report an electronic cloaking effect as a manifestation of chirality by probing phase coherent transport in chemical-vapor-deposited bilayer graphene. Conductance oscillations with different periodicities were observed on extremely narrow bilayer graphene heterojunctions through electrostatic gating. Using a Fourier analysis technique, we identified the origin of each individual interference pattern. Importantly, the electron waves on the two sides of the potential barrier can be coupled through the evanescent waves inside the barrier, making the confined states underneath the barrier invisible to electrons. These findings provide direct evidence for the electronic cloaking effect and hold promise for the realization of pseudospintronics based on bilayer graphene.

DOI: 10.1103/PhysRevB.94.205418

Since the experimental observation of unconventional integer quantum Hall effects [1–3] in monolayer graphene, chirality has been considered to have a key role in understanding unusual transport behaviors of massless Dirac fermions [4–8]. One prime example is Klein tunneling, characterized by perfect transmission through the barrier regardless of its width and energy height [5,9–19]. Different from monolayer graphene, charge carriers in bilayer graphene (BLG) are massive Dirac fermions also with a chiral nature, but a finite density of states at zero energy [5,9,20,21]. The case of chiral tunneling in BLG bipolar junctions is intriguing [22–24], where complete decoupling between quasiparticle states of opposite polarity has been predicted theoretically at normal incidence due to chirality mismatch [9,23–25]. A striking consequence of chirality mismatch is the rendering of confined states via a potential barrier from opposite pseudospin states invisible to electron transport—the so-called electronic cloaking effect [23]. This electronic cloaking is different from optical cloaking in the sense that the probing waves directly tunnel through the potential barrier where cloaked states are contained, not by moving around cloaked objects as in the optical cloaking effect [23,26,27]. However, experimental verification of the electronic cloaking effect is still challenging. To this end, we present experimental evidence of electronic cloaking and Klein tunneling of massive Dirac fermions in BLG by probing the phase coherent transport behavior of a dual-gated BLG transistor.

The devices were fabricated on chemical-vapor-deposited bilayer graphene with channel lengths between 50 to 200 nm [28] (see Supplemental Material [29] for detail). The schematic and a scanning electron microscopy image of representative devices are shown in Figs. 1(a) and 1(b). In contrast to earlier implementation of a dual-gated devices, which induced Fabry-Perot interference only inside a potential barrier [13,30,31], the dual-gated BLG device described here allows a phase coherent transport regime over the full channel length, which is a necessary condition to realize electronic cloaking phenomena. This approach allows us to prevent loss of phase information when charge carriers traverse the BLG channel.

Conductance oscillations arising from Fabry-Perot interference in these BLG devices can originate from several possible trajectories related to the chiral massive fermions. We first look at the monopolar regime Fig. 1(c). Graphene underneath the source and drain metal contacts can be doped by charge transfer from metals and may have a different polarity from that of the channel region [32,33]. Fabry-Perot interference can appear with a resonance cavity length defined by the effective channel length of the device Fig. 1(c) [13,33–35].

In a more sophisticated way, the bipolar regime, where the polarity of graphene regions controlled by the back gate and the top gate are different, can offer an opportunity to unravel the crucial role of chirality in transport through the potential barrier [13,14,16–18]. As shown in Fig. 1(d), conductance oscillations can arise from electron (blue arrow) and hole (yellow arrow) round-trip resonances confined within the back-gate-controlled left and right graphene regions, and center region controlled by both top and back gates. More interestingly, chiral carriers could have an additional possible route to complete a round trip across the potential barrier via quantum tunneling (green arrow), as if the confined states underneath the barrier are invisible to the carrier transport. At normal incidence, the coupling between the positive and negative energy states is completely suppressed due to pseudospin conservation in bilayer graphene, in which chirality is tied to the polarity of charge carriers [9,23]. The quasiparticle states on both sides of the barrier, however, have the same pseudospin and can be coupled via evanescent waves. As a result, the potential barrier acts as a cloak for the confined

*zzhong@umich.edu

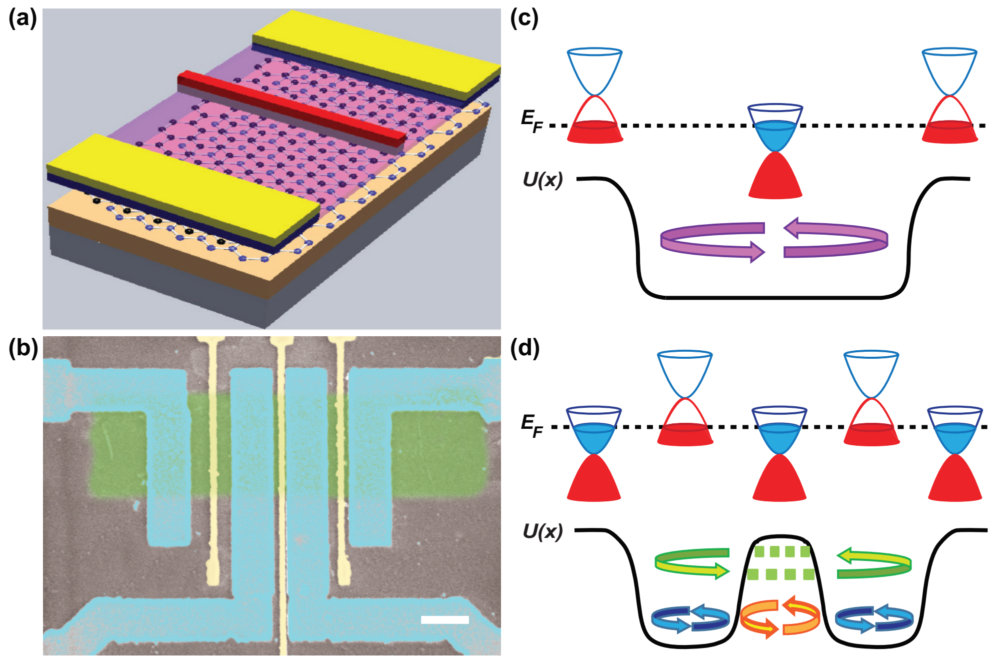

FIG. 1. (a) Schematic diagram of a dual-gated BLG device. (b) False-color scanning electron microscopy image of three BLG devices having different channel lengths (200, 50, and 100 nm from left to right). Source/drain electrodes, BLG, and top-gate electrodes are represented by blue, green, and yellow color, respectively. The scale bar is 200 nm. (c) Schematic showing Fabry-Perot resonance in monopolar regime due to reflection at the source and drain contact. (d) Schematic illustration of electronic cloaking resonance in BLG arising from decoupling of orthogonal pseudospins in bipolar regime (green color). Blue- and yellow-colored trajectories show resonance of confined states by potential barrier.

states underneath with opposite pseudospin, rendering them invisible to the massive Dirac fermion transport across the barrier. The observation of resonance across the entire device in the bipolar regime will thus provide strong proof for the intriguing electronic cloaking effect in BLG.

We first characterize carrier transport in single back-gated BLG devices via two-terminal measurements at 6 K. Figure 2(a) shows the two-dimensional (2D) color plot of differential conductance as a function of back-gate voltage (V_{BG}) and bias voltage (V) for a device with 55 nm channel length. The smooth background is subtracted to enhance the periodic patterns. Chessboard patterns are clearly visible in the 2D plot, with the quasiperiodic patterns highlighted by the guide lines. Similar periodic features can also be observed in devices with 118 nm and 160 nm channel lengths Figs. 2(b) and 2(c). These results are in agreement with the Fabry-Perot–like quantum interference of electron waves [13,34,35].

The observed quantum interference can be understood by examining the round-trip resonance condition. Whenever the phase change obtained by the round trip of an electron reaches 2π, a constructive interference pattern appears for $\Delta k_F = \pi/L$. Combining this condition with parabolic band dispersion of BLG gives

$$eV_C = \frac{\hbar^2 \pi C_{\mathrm{BG}} \Delta V_{\mathrm{BG}}}{2m^*} = \frac{\hbar^2}{m^*}\left[\left(\frac{\pi}{W}\right)^2 + \left(\frac{\pi}{L}\right)^2\right] \approx \frac{\hbar^2 \pi^2}{m^* L^2} \tag{1}$$

where m^* is the effective mass having $0.03m_e$ [34], and C_{BG} is the gate capacitance, which is equal to $175\,\mathrm{nF/cm^2}$ as calculated according to the parallel plate capacitor model. We note that here we only consider the lowest-energy mode of Fabry-Perot oscillation. The oscillation periods, in eV_{C}, scale inversely with the square of the channel length (L) for BLG. In comparison, for single-layer graphene, due to its linear band dispersion, the eV_{C} is expected to be inversely proportional to L. Moreover, the gate voltage oscillation period (ΔV_{BG}) is similar at low and high carrier density for BLG, whereas ΔV_{BG} changes significantly as gate voltage varies for single-layer graphene [34]. We further extracted the bias voltage oscillation period (V_{C}) and gate voltage oscillation period (ΔV_{BG}), respectively, for three devices: 21 (± 2) mV, 0.45 (± 0.02) V for the $L = 55$ nm device; 5.1 (± 0.3) mV and 0.12 (± 0.02) V for the $L = 118$ nm device; 3.1 (± 0.1) mV and 0.065 (± 0.02) V for the $L = 160$ nm device. As shown in Fig. 2(d), the measured eV_{C} scales inversely with L^2, and the small deviation can be attributed to the fact that the resonance cavity length is smaller than its physical length due to the fringing field screening effect from the metal electrodes [36]. We estimate a resonance cavity length of 50 nm for the device with 55 nm physical length. These results also indicate that the phase coherence length in our chemical-vapor-deposited BLG is larger than 160 nm.

To study the anomalous chiral electron tunneling behavior, we now focus on the transport measurements of the dual-gated BLG devices, starting with a 150-nm-channel-length device. The differential resistance is measured as a function of back and top gate voltages. Figure 3(a) shows the 2D color plot of the resistance, and the four quadrants correspond to the monopolar ($n-n-n$ and $p-p-p$) and bipolar regimes ($p-n-p$ and $n-p-n$). The slope of the charge-neutral line gives the capacitive coupling ratio between the top gate and back gate,

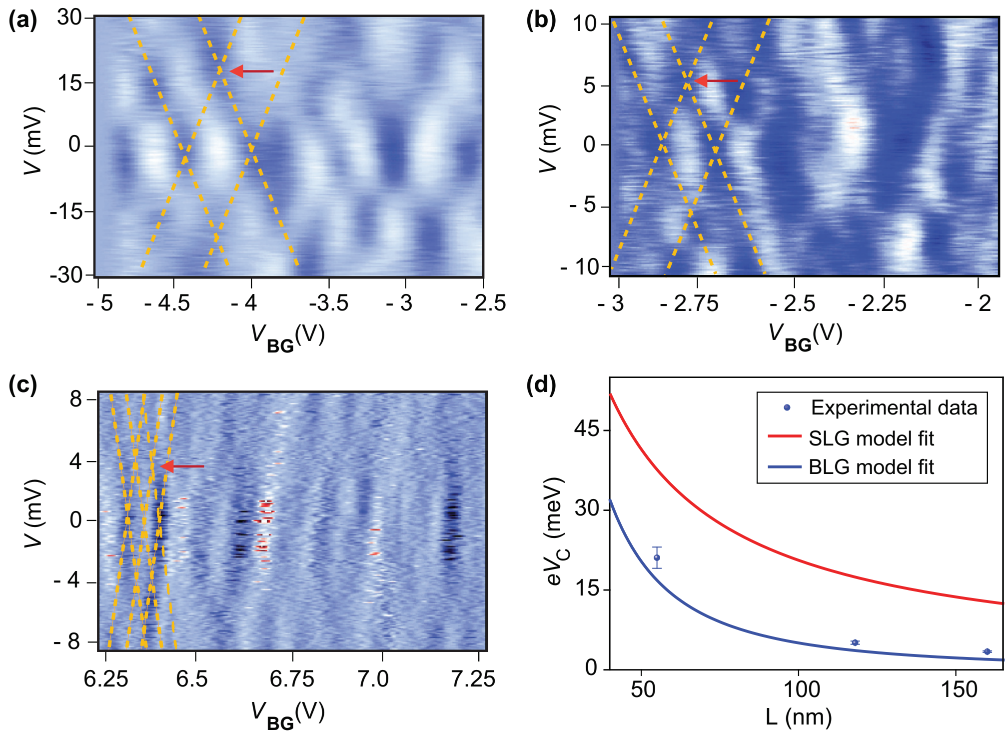

FIG. 2. Fabry-Perot resonance in back-gated BLG devices. (a), (b), and (c), Two-dimensional color plot of differential conductance versus V and V_{BG} for BLG device with channel length of (a) 55 nm, (b) 118 nm, and (c) 160 nm. The channel width is 500 nm for all three devices, and all data are taken at 6 K. For each image, a smooth background was subtracted to highlight the Fabry-Perot oscillation patterns. Quasiperiodic crisscrossing dark (bright) lines correspond to conductance dips (peaks). The dotted yellow lines are guides to the eye, and the red arrows indicate the bias voltage oscillation period (V_C). (d) eV_C measured from three devices plotted against device physical channel length. The results are also compared with theoretical length-dependent resonance periods for single-layer graphene with linear dispersion (red curve) and BLG with parabolic dispersion (blue curve).

$C_{TG}/C_{BG} \sim 1.7$. A rich set of oscillatory features is observed in this differential resistance map: one interference pattern in the monopolar regime, and more than two fringes forming checkerboard-like complex interference patterns in the bipolar regime.

In order to understand the origin of the resonances and gain a better insight into the transport mechanism, we employed a 2D fast Fourier transform (FFT) analysis technique for extracting the interference patterns [37]. The main role of the 2D FFT technique is to separate fringe patterns affected by different combinations of top- and back-gate voltages along the horizontal (N_B) and diagonal (N_T) orientations. By masking one fringe pattern and performing inverse FFT on the other fringe patterns, we can clarify the presence of two different fringe components along each orientation Figs. 3(b) and 3(c). The summation of these separated fringe patterns recovers the original 2D differential resistance map with more pronounced interference patterns Fig. 3(d).

The FFT filtered data sets enable us to better understand the observed interference patterns. We first examine the resonances along the N_T orientation as shown in Fig. 3(b). In the monopolar region, sequences of periodic oscillations are clearly visible as indicated by the purple line. The FFT along V_{BG} in the monopolar region shows a peak frequency at 16.39 (1/V), corresponding to an oscillation period of $\Delta V_{BG} \sim 0.061$ V (see Fig. S2). Using Eq. (1), this value corresponds to a BLG resonator cavity length of ~138 nm, in agreement with the physical length between source and drain electrodes (150 nm). By calculating the mobility as $\mu = \frac{\sigma}{ne}$ and the mean free path as $l_e = \frac{h}{e^2}\frac{\sigma}{2\sqrt{\pi n}}$, we estimated carrier mobility $\mu \sim 4000\,\mathrm{cm}^2\,\mathrm{V}^{-1}\,\mathrm{s}^{-1}$ with $l_e \sim 82$ nm at a carrier density of $3 \times 10^{12}\,\mathrm{cm}^{-2}$. We note that this value represents the lower-bound mean free path without removing the effect of contact resistance [38].

We now turn our attention to the bipolar region. Oscillations along the N_T direction with different periodicities are clearly present, as highlighted by the green and dotted yellow lines in Fig. 3(b). The FFT analysis in the bipolar region Fig. 3(e) yields two primary oscillation periods of 0.270 V and 0.151–0.189 V, which correspond to a resonant cavity length of 65 nm and 78–87 nm, respectively. The cavity length of 65 nm is in reasonable agreement with the fabricated top-gate width of 30 nm, taking into account the smooth potential profile [13,14,16,39] due to the estimated width of the $p-n$ junction, which is ~18 nm (see Fig. S3). This result is consistent with the existence of a localized state confined underneath the top gate by potential barriers yellow arrows in Fig. 3(b) inset.

The second oscillation, corresponding to cavity sizes of 78–87 nm, is more intriguing. The resonant condition for these cavities immediately invites one to consider electrons bouncing back and forth within graphene sections between top-gate and metal electrodes—states confined in either the left or right BLG lead regions. However, we rule out this

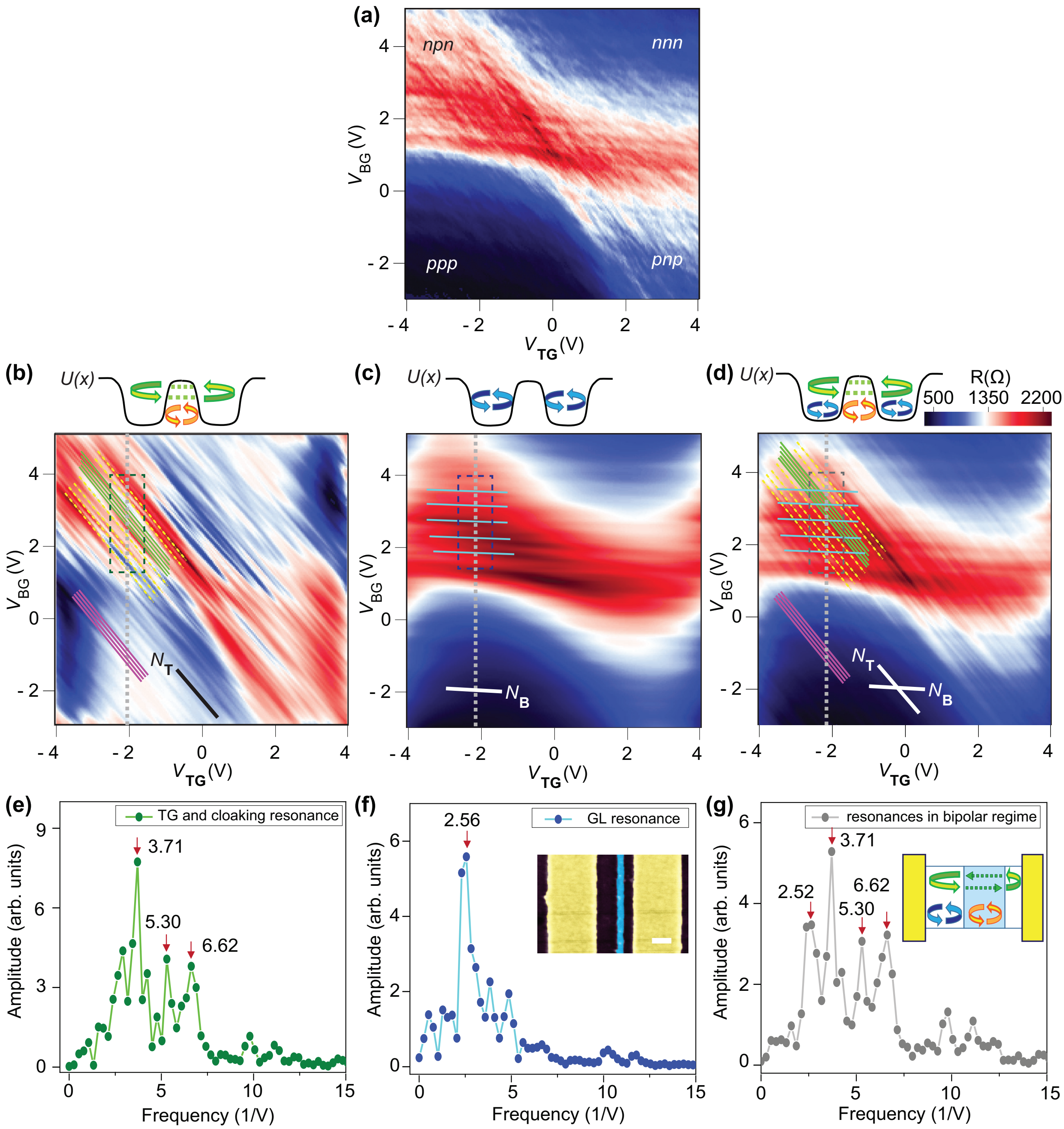

FIG. 3. Electronic cloaking effect in dual-gated BLG device. (a) Two-dimensional resistance map as a function of V_{TG} and V_{BG} from a 150 nm BLG device. (b) and (c) To extract oscillation components controlled by both V_{TG} and V_{BG}, and controlled only by V_{BG} separately, inverse Fourier transform with masking technique was performed on the 2D resistance map in (a). The two fringing patterns along the (b) N_T (black solid line) and (c) N_B directions (white solid line) were obtained, respectively. (d) Two-dimensional resistance map is recovered with clearer oscillation patterns by adding two fringing patterns, (b) and (c). Top insets in (b), (c), (d) show representative trajectories for each resonance condition. Observed Fabry-Perot conductance oscillations are represented by yellow, green, and blue lines, respectively in (b), (c), (d), corresponding to massive Dirac fermion trajectories with the same colors shown in the insets. (e), (f), (g) The Fourier transform spectra for (b), (c), and (d), respectively. The Fourier transforms were performed along the gray dashed line ($V_{TG} = -2.1$ V) in the highlighted dashed square regions. Note that weak higher harmonics are also observed, corresponding to multiple rotating trajectories within the defined cavities. The inset in (f) shows false-color SEM image of a device with top gate (blue), source-drain electrodes (yellow), and BLG (dark purple). The scale bar is 100 nm. The schematic view of resonant cavity lengths with trajectories is drawn for corresponding FFT results in the inset in (g).

TABLE I. Physical lengths and resonance cavity lengths estimated from oscillation periods (ΔV_{BG}) in the studied BLG devices. TG is top-gate and GL is graphene lead.

Channel Length			TG			GL			Cloaking	
	Resonant cavity			Resonant cavity			Resonant cavity		Resonant cavity	
Physical [nm]	[nm]	$\Delta V_{\rm BG}$(mV)	Physical [nm]	[nm]	$\Delta V_{\rm BG}$(mV)	Physical [nm]	[nm]	$\Delta V_{\rm BG}$(mV)	[nm]	$\Delta V_{\rm BG}$(mV)
150	136 ± 3.2	60 ± 3	30	64.4 ± 2.5	280 ± 20	80	54 ± 2.2	390 ± 30	82.3 ± 3.5	170 ± 10
120	109 ± 8	98 ± 15	30	50.1 ± 5	470 ± 90	60	50.2 ± 4.4	460 ± 70	74.6 ± 3.2	210 ± 20
100	94 ± 7	130 ± 20	30	44 ± 3.3	640 ± 110	50	37.7 ± 3.7	830 ± 160	58.3 ± 3.7	340 ± 40

possibility because (1) the density of carriers localized in the BLG leads can only be tuned by back-gate voltage, not by top-gate voltage [40], and (2) the length of the resonant cavity (78–87 nm) is also larger than the resonant cavity length of the left and right BLG leads (∼60 nm) by considering the width of the $p-n$ junction (∼18 nm). The other plausible explanation is that plane waves, either on the left or right side of the potential barriers, are coupled through the evanescent waves inside the barrier, as if there are no available states under the barrier (green arrows in Fig. 3(b) inset). Note that the energy of normally incident quasiparticle waves is slightly lower than the barrier height, but it is high enough to tunnel through the barrier, for the realization of the cloaking effect. Otherwise, this condition is not satisfied, since the tunneling probability decreases significantly as energy difference increases between quasiparticle waves and the barrier height. The observation of resonance mode with trajectory bouncing through the full device is highly unusual, thus demonstrating that the necessary condition is fulfilled. Indeed, the value of full channel length (∼150 nm) approximately equals the sum of the resonant cavity length defined by the top gate (∼65 nm) and the quasiparticle propagation distance (78–87 nm). The results thus provide experimental evidence for the electronic cloaking effect due to the pseudospin mismatch of opposite polarity. The discrepancy of propagation distance, ∼9 nm, is attributed to the variation in the potential profile as back-gate voltage sweeps. The splitting of the resonant peak in the FFT analysis can be understood in the context of this potential variation. This interpretation was carefully investigated by identification of corresponding oscillations in the original 2D color map, and it was also confirmed with density profiles using finite-element simulation software (Fig. S3). The rather small variation in the potential profile seems to be due to electric field screening of back-gate by top-gate, source, and drain metal electrodes in our BLG nanostructures [31,41,42].

We also studied the oscillations along the $N_{\rm B}$ direction Fig. 3(c), where periodic resonance is clearly visible in the bipolar region. The FFT spectrum Fig. 3(f) taken from the data along the dashed line in Fig. 3c show an oscillation period of 0.391 V, corresponding to a resonant cavity length of 54 nm. The resonant cavity length is consistent with the physical length of left BLG lead (∼80 nm, Fig. 3f inset), taking account of the width of the $p-n$ junction (∼18 nm) due to the smooth potential profile. The result indicates that a significant fraction of near normally incident waves with energy much smaller than the barrier height is reflected at the interface of the $p-n$ junction. Given the confined states underneath the top gate, we attribute this feature to chirality mismatch leading to the suppression of electron-hole coupling, a consequence of the anti-Klein tunneling effect [9]. Regarding the resonant cavity of the right BLG lead, the expected quantum interference was not observed, either on FFT or on the 2D resistance map, due to the fact that the oscillation period seems to be beyond our detection limit, i.e., ∼2 V, in terms of back-gate voltage Figs. 3(f) inset and 3(g) inset. The slight asymmetry of the right and left BLG leads is due to the shift of the top gate by 15–20 nm, as confirmed from the SEM image Fig. 3(f) inset.

We now note that the cloaking resonance cavity should be equal to the sum of the resonant cavity lengths of the left and right BLG leads. Even though the measured oscillation peak was not found for the right BLG lead cavity, we can still estimate the resonant cavity size (∼22 nm) by subtracting the width of the $p-n$ junction from the physical length of the right BLG lead (∼40 nm) determined from the SEM image Fig. 3(f) inset. Given this, and in light of the analysis on cloaking cavity, the sum of the estimated resonant cavity length of the left and right BLG leads, 76 nm, is still quantitatively in good agreement with the cloaking cavity size, within error range (≈ 10 nm), owing to the potential profile variation as back-gate voltage changes. Such remarkable agreement provides further evidence that the observed cloaking resonance, during the full round trip across the BLG channel by tunneling the barrier, results from coupling between quasiparticles with the same pseudospin orientation.

Similar quantum interference phenomena were observed from other devices with 120 nm and 100 nm channel length, respectively (see Supplemental Material [29]). Importantly, in the bipolar region, they also showed oscillation features corresponding to (1) the resonance cavity defined by the top gate, and (2) a "cloaking cavity" extended throughout the whole device, with states underneath the top gate invisible. For all samples, we carefully recorded FFT results along vertical lines at 10 different top-gate voltages within the highlighted dashed square regions both at bipolar and monopolar regimes (Table I). As such, we also identified low-frequency peaks as noise signals Figs. 3(e), 3(f), and 3(g), because these were not repetitively present at different FFT results, and the corresponding periods were not identified in the original 2D resistance map. The results from all three devices paint a consistent picture of different types of quantum interference due to the chiral nature of massive Dirac fermions, as depicted in Fig. 1(d).

In conclusion, we present experimental evidence of the electronic cloaking effect by probing phase coherent transport behavior in our chemical-vapor-deposited BLG devices. Further evidence can come from magnetic field–dependent studies [13,31], and by fabricating devices on hexagonal boron nitride (h-BN) substrates [19,43] to achieve much longer phase coherence length. The results support the utilization of chiral-dependent transport properties to encode information using pseudospins of massive fermions, and they may pave the way for future applications of pseudospintronics with bilayer graphene.

We thank J. Song and L. Levitov for their helpful discussions. This work was supported by the National Science Foundation (NSF) Scalable Nanomanufacturing Program (DMR-1120187). Z.Z. acknowledges support from the NSF CAREER Award (ECCS-1254468). K.L. acknowledges support from the Kwanjeong Educational Foundation. Devices were fabricated in the Lurie Nanofabrication Facility at the University of Michigan, a member of the NSF National Nanotechnology Infrastructure Network.

[1] K. S. Novoselov, Z. Jiang, Y. Zhang, S. V. Morozov, H. L. Stormer, U. Zeitler, J. C. Maan, G. S. Boebinger, P. Kim, and A. K. Geim, Science **315**, 1379 (2007).
[2] K. S. Novoselov, A. K. Geim, S. V. Morozov, D. Jiang, M. I. Katsnelson, I. V. Grigorieva, S. V. Dubonos, and A. A. Firsov, Nature **438**, 197 (2005).
[3] Y. Zhang, Y.-W. Tan, H. L. Stormer, and P. Kim, Nature **438**, 201 (2005).
[4] C. W. J. Beenakker, Rev. Mod. Phys. **80**, 1337 (2008).
[5] A. K. Geim and K. S. Novoselov, Nat. Mater. **6**, 183 (2007).
[6] C. W. J. Beenakker, Phys. Rev. Lett. **97**, 067007 (2006).
[7] V. V. Cheianov, V. Fal'ko, and B. L. Altshuler, Science **315**, 1252 (2007).
[8] A. Rycerz, J. Tworzydlo, and C. W. J. Beenakker, Nat. Phys. **3**, 172 (2007).
[9] M. I. Katsnelson, K. S. Novoselov, and A. K. Geim, Nat. Phys. **2**, 620 (2006).
[10] T. Ando, T. Nakanishi, and R. Saito, J. Phys. Soc. Jpn. **67**, 2857 (1998).
[11] O. Klein, Zeitschrift für Physik **53**, 157 (1929).
[12] T. Tudorovskiy, K. J. A. Reijnders, and M. I. Katsnelson, Phys. Scr. **T146**, 014010 (2012).
[13] A. F. Young and P. Kim, Nat. Phys. **5**, 222 (2009).
[14] R. V. Gorbachev, A. S. Mayorov, A. K. Savchenko, D. W. Horsell, and F. Guinea, Nano Lett. **8**, 1995 (2008).
[15] V. V. Cheianov and V. I. Fal'ko, Phys. Rev. B **74**, 041403 (2006).
[16] B. Huard, J. A. Sulpizio, N. Stander, K. Todd, B. Yang, and D. Goldhaber-Gordon, Phys. Rev. Lett. **98**, 236803 (2007).
[17] N. Stander, B. Huard, and D. Goldhaber-Gordon, Phys. Rev. Lett. **102**, 026807 (2009).
[18] A. V. Shytov, M. S. Rudner, and L. S. Levitov, Phys. Rev. Lett. **101**, 156804 (2008).
[19] P. Rickhaus, R. Maurand, M.-H. Liu, M. Weiss, K. Richter, and C. Schönenberger, Nat. Commun. **4**, 2342 (2013).
[20] E. McCann and V. I. Fal'ko, Phys. Rev. Lett. **96**, 086805 (2006).
[21] K. S. Novoselov, E. McCann, S. V. Morozov, V. I. Fal'ko, M. I. Katsnelson, U. Zeitler, D. Jiang, F. Schedin, and A. K. Geim, Nat. Phys. **2**, 177 (2006).
[22] R. Nandkishore and L. Levitov, Proc. Natl. Acad. Sci. USA **108**, 14021 (2011).
[23] N. Gu, M. Rudner, and L. Levitov, Phys. Rev. Lett. **107**, 156603 (2011).
[24] V. Kleptsyn, A. Okunev, I. Schurov, D. Zubov, and M. I. Katsnelson, Phys. Rev. B **92**, 165407 (2015).
[25] S. Park and H. S. Sim, Phys. Rev. B **84**, 235432 (2011).
[26] D. Schurig, J. J. Mock, B. J. Justice, S. A. Cummer, J. B. Pendry, A. F. Starr, and D. R. Smith, Science **314**, 977 (2006).
[27] U. Leonhardt, Science **312**, 1777 (2006).
[28] S. Lee, K. Lee, and Z. Zhong, Nano Lett. **10**, 4702 (2010).
[29] See Supplemental Material at http://link.aps.org/supplemental/10.1103/PhysRevB.94.205418 for device fabrication and electronic cloaking effects from 100 nm/120 nm channel length BLG devices.
[30] L. C. Campos, A. F. Young, K. Surakitbovorn, K. Watanabe, T. Taniguchi, and P. Jarillo-Herrero, Nat. Commun. **3**, 1239 (2012).
[31] A. Varlet, M.-H. Liu, V. Krueckl, D. Bischoff, P. Simonet, K. Watanabe, T. Taniguchi, K. Richter, K. Ensslin, and T. Ihn, Phys. Rev. Lett. **113**, 116601 (2014).
[32] P. A. Khomyakov, A. A. Starikov, G. Brocks, and P. J. Kelly, Phys. Rev. B **82**, 115437 (2010).
[33] Y. Wu, V. Perebeinos, Y.-m. Lin, T. Low, F. Xia, and P. Avouris, Nano Lett. **12**, 1417 (2012).
[34] S. Cho and M. Fuhrer, Nano Res. **4**, 385 (2011).
[35] W. Liang, M. Bockrath, D. Bozovic, J. H. Hafner, M. Tinkham, and H. Park, Nature **411**, 665 (2001).
[36] Y.-M. Lin, J. Appenzeller, and P. Avouris, Nano Lett. **4**, 947 (2004).
[37] N. M. Gabor, J. C. W. Song, Q. Ma, N. L. Nair, T. Taychatanapat, K. Watanabe, T. Taniguchi, L. S. Levitov, and P. Jarillo-Herrero, Science **334**, 648 (2011).
[38] E. Vogel, A. Venugopal, and L. Colombo, ECS Transactions **35**, 229 (2011).
[39] P. E. Allain and J. N. Fuchs, Eur. Phys. J. B **83**, 301 (2011).
[40] B. Özyilmaz, P. Jarillo-Herrero, D. Efetov, D. A. Abanin, L. S. Levitov, and P. Kim, Phys. Rev. Lett. **99**, 166804 (2007).
[41] N. Seung-Geol, K. Dong-Keun, P. Jong Wan, K. Youngwook, K. Jun Sung, and L. Hu-Jong, Nanotechnology **22**, 415203 (2011).
[42] A. Barreiro, H. S. J. van der Zant, and L. M. K. Vandersypen, Nano Lett. **12**, 6096 (2012).
[43] C. R. Dean, A. F. Young, I. Meric, C. Lee, L. Wang, S. Sorgenfrei, K. Watanabe, T. Taniguchi, P. Kim, K. L. Shepard, and J. Hone, Nat. Nanotechnol. **5**, 722 (2010).